

## Electronic spectroscopy and electronic structure of diatomic TiFe

Olha Krechkivska, Michael D. Morse, Apostolos Kalemos, and Aristides Mavridis

Citation: *J. Chem. Phys.* **137**, 054302 (2012); doi: 10.1063/1.4738958

View online: <http://dx.doi.org/10.1063/1.4738958>

View Table of Contents: <http://jcp.aip.org/resource/1/JCPSA6/v137/i5>

Published by the American Institute of Physics.

---

### Additional information on J. Chem. Phys.

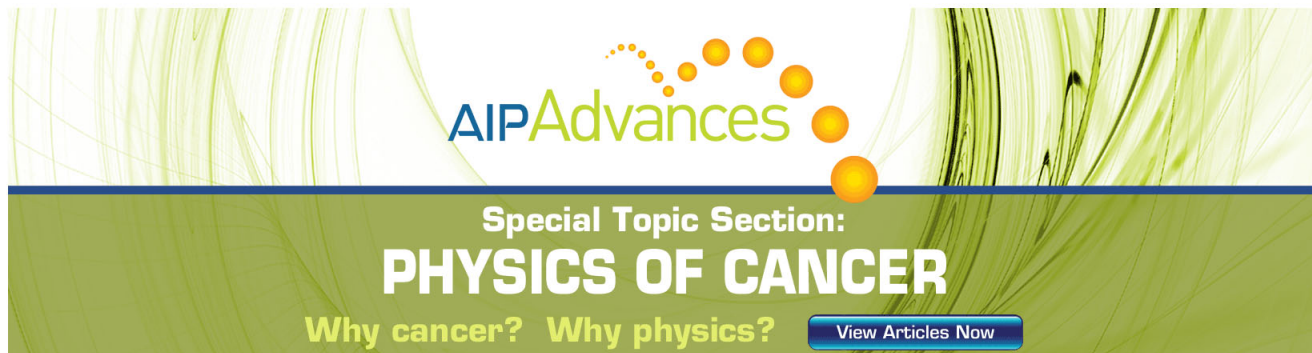
Journal Homepage: <http://jcp.aip.org/>

Journal Information: [http://jcp.aip.org/about/about\\_the\\_journal](http://jcp.aip.org/about/about_the_journal)

Top downloads: [http://jcp.aip.org/features/most\\_downloaded](http://jcp.aip.org/features/most_downloaded)

Information for Authors: <http://jcp.aip.org/authors>

## ADVERTISEMENT



**AIPAdvances**

Special Topic Section:  
**PHYSICS OF CANCER**

Why cancer? Why physics? [View Articles Now](#)

# Electronic spectroscopy and electronic structure of diatomic TiFe

Olha Krechkivska,<sup>1</sup> Michael D. Morse,<sup>1,a)</sup> Apostolos Kalamos,<sup>2</sup> and Aristides Mavridis<sup>2</sup><sup>1</sup>Department of Chemistry, University of Utah, Salt Lake City, Utah 84112, USA<sup>2</sup>Department of Chemistry, Laboratory of Physical Chemistry, National and Kapodistrian University of Athens, Athens 157 71, Greece

(Received 16 May 2012; accepted 10 July 2012; published online 1 August 2012)

Diatomic TiFe, a 12 valence electron molecule that is isoelectronic with Cr<sub>2</sub>, has been spectroscopically investigated for the first time. In addition, the first computational study that includes the ground and excited electronic states is reported. Like Cr<sub>2</sub>, TiFe has a  $^1\Sigma^+$  ground state that is dominated by the  $1\sigma^2 2\sigma^2 1\pi^4 1\delta^4$  configuration. Rotationally resolved spectroscopy has established a ground state bond length of 1.7024(3) Å, quite similar to that found for Cr<sub>2</sub> ( $r_0 = 1.6858$  Å). Evidently, TiFe exhibits a high degree of multiple bonding. The vibronic spectrum is highly congested and intense to the blue of 20 000 cm<sup>-1</sup>, while two extremely weak band systems, the  $[15.9]^3\Pi_1 \leftarrow X^1\Sigma^+$  and  $[16.2]^3\Pi_{0+} \leftarrow X^1\Sigma^+$  systems, are found in the 16 000–18 500 cm<sup>-1</sup> region. The bond lengths, obtained by inversion of the  $B_e'$  values, and vibrational frequencies of the two upper states are nearly identical: 1.886 Å and 344 cm<sup>-1</sup> for  $[15.9]^3\Pi_1$  and 1.884 Å and 349 cm<sup>-1</sup> for  $[16.2]^3\Pi_{0+}$ . The measured spin-orbit splitting of the  $^3\Pi$  state is consistent with its assignment to the  $1\sigma^2 2\sigma^2 1\pi^4 1\delta^3 2\pi^1$  configuration, as is also found in the *ab initio* calculations. © 2012 American Institute of Physics. [<http://dx.doi.org/10.1063/1.4738958>]

## I. INTRODUCTION

Among the diatomic transition metals, Cr<sub>2</sub> occupies a position of particular prominence because of early controversies concerning its ground state potential curve, especially as regards the bond length. With ground state atoms having configurations of  $3d^5 4s^1$ ,  $^7S$ , it is possible in principle to spin-pair all 12 valence electrons in Cr<sub>2</sub>, placing them in  $s\sigma_g$ ,  $d\sigma_g$ ,  $d\pi_u$ , and  $d\delta_g$  bonding orbitals to form a tightly bound diatomic molecule with a nominal sextuple bond. This intriguing possibility has sparked a large experimental and computational effort.

On the experimental side, the first spectrum of Cr<sub>2</sub> was obtained in 1974 in a transient absorption study of the products formed in a flash photolysis experiment on gaseous Cr(CO)<sub>6</sub>.<sup>1</sup> The spectrum was assigned to a  $^1\Sigma_u^+ \leftarrow X^1\Sigma_g^+$  transition in diatomic Cr<sub>2</sub>, for which a bond length of 1.71 Å was found. However, the possibility that the carrier of the spectrum might be linear CrO<sub>2</sub> or CrC<sub>2</sub> was not rigorously excluded. Subsequently, the molecule was investigated by matrix isolation absorption and emission<sup>2–4</sup> and Raman spectroscopy,<sup>5–7</sup> and by laser-induced fluorescence<sup>8,9</sup> and resonant two-photon ionization spectroscopy<sup>10</sup> in jet-cooled molecular beams. While these results have shown that the  $^1\Sigma_g^+$  ground state of Cr<sub>2</sub> has a short bond length with  $r_e = 1.6788$  Å,<sup>8</sup> details of the shape of the potential energy surface did not emerge until the photoelectron spectrum of mass-selected Cr<sub>2</sub><sup>-</sup> was measured in 1991. This study revealed a tight potential curve near the bottom of the well that seems to approach a dissociation limit at longer distances as the d-orbital bonds are broken, but which then rises again to the

true dissociation limit at even longer distances as the s-orbital bond is broken.<sup>11</sup>

Computational chemistry has found Cr<sub>2</sub> to be very challenging, owing to the large exchange effects that result from the small size of the  $3d^5$  subshell and the high degree of electron correlation in the molecule. An early MCSCF calculation found Cr<sub>2</sub> to have a bond length of 3.06 Å dominated by s-orbital bonding,<sup>12</sup> while a subsequent calculation on the isovalent Mo<sub>2</sub> found a double minimum, in which the molecule could exist in either a long-bonded form dominated by s-orbital bonding or as a short-bonded form in a deeper d-bonded well.<sup>13</sup> This led to the speculation that Cr<sub>2</sub> might exhibit a double-minimum potential curve in the ground state, prompting the photoelectron study mentioned above. As a result of the computational difficulties inherent in a study of Cr<sub>2</sub>, it has become a standard test molecule for all newly developed electronic structure methods.<sup>14–53</sup>

It is interesting to consider how the electronic structure of Cr<sub>2</sub> may change, as one proceeds along an isoelectronic sequence that redistributes charge from one nucleus to the other. We may define our position on this isoelectronic sequence in terms of the nuclear charge asymmetry, defined by  $\Delta Z = |Z_A - Z_B|$ . It is now known that Cr<sub>2</sub> ( $\Delta Z = 0$ ) has a very short bond with a high degree of multiple bonding character. How does this change in moving to VMn ( $\Delta Z = 2$ ), TiFe ( $\Delta Z = 4$ ), ScCo ( $\Delta Z = 6$ ), CaNi ( $\Delta Z = 8$ ), KCu ( $\Delta Z = 10$ ), and ArZn ( $\Delta Z = 12$ )? Does the bond strength decrease and the bond length increase smoothly as one moves along this sequence, or are there break points where the nature of the bonding changes abruptly? Among the multiply bonded p-block molecules, N<sub>2</sub> ( $\Delta Z = 0$ ,  $r_e = 1.0977$  Å,  $\omega_e = 2358.6$  cm<sup>-1</sup>) (Ref. 54) and CO ( $\Delta Z = 2$ ,  $r_e = 1.1283$  Å,  $\omega_e = 2169.8$  cm<sup>-1</sup>) (Ref. 54) are uniformly considered to have triple bonds that are well-described by the simple Lewis dot

<sup>a)</sup> Author to whom correspondence should be addressed. Electronic mail: [morse@chem.utah.edu](mailto:morse@chem.utah.edu). FAX: (801)-581-8433.

structures,  $\text{:N}\equiv\text{N:}$  and  $\text{:C}\equiv\text{O:}$ . Diatomic BF ( $\Delta Z = 4$ ,  $r_e = 1.2626 \text{ \AA}$ ,  $\omega_e = 1402.1 \text{ cm}^{-1}$ ) (Ref. 54) begins to show a somewhat different electronic structure, with a significantly longer bond, a significantly lower vibrational frequency, and much greater ionic contributions to the bond. By the time one reaches BeNe, no chemist would describe this species as having a triply bonded  $\text{:Be}\equiv\text{Ne:}$  structure; indeed, BeNe is for all practical purposes unbound.

The lack of corresponding data on the transition metal species has prompted this investigation on diatomic TiFe. No previous spectroscopic data exist for this molecule, and only one density functional theory (DFT) study has been previously reported.<sup>55</sup> In order to rectify this situation, and learn how the electronic structure is modified as the nuclear charge is made more asymmetric in these 12-electron molecules, we have undertaken spectroscopic and computational studies of diatomic TiFe. A previous study of the isovalent molecule, ZrFe, has already been reported.<sup>56</sup>

In Sec. II we present a description of the experimental methods that were employed in this study, while Sec. III provides details of the computational methods. Experimental results are provided in Sec. IV and the results of the theoretical investigation are given in Sec. V. Finally, the most important findings are summarized in Sec. VI.

## II. EXPERIMENTAL METHODS

In the present study, diatomic TiFe was investigated by means of resonant two-photon ionization spectroscopy (R2PI). The instrument employed in this work is identical to that used in our recent investigation of the isovalent ZrFe molecule,<sup>56</sup> and is therefore only briefly described. Diatomic TiFe is produced by focusing the fundamental radiation from a Q-switched Nd:YAG laser (1064 nm, 25–30 mJ/pulse) onto a Ti:Fe 1:1 alloy (ACI Alloys) in the throat of a pulsed supersonic expansion of helium (180–200 psi backing pressure). The alloy sample is in the form of a disk that is rotated and translated to prevent the drilling of a deep hole into the sample, thereby maintaining a nearly constant TiFe concentration in the resulting molecular beam. After supersonic expansion into the source chamber, the molecular beam passes through a skimmer (50° inside angle, 1.5 cm diameter) that provides a roughly collimated beam in the second chamber, which is the ionization region of a linear time-of-flight mass spectrometer.

In the second chamber, the molecular beam is exposed to unfocused radiation emitted by a Nd:YAG pumped dye laser that is counterpropagated along the molecular beam axis. After a few tens of nanoseconds, the 5th harmonic output of a Nd:YAG laser (212.8 nm, 5–6 mJ/pulse) is directed across the molecular beam axis at right angles. Neither wavelength is capable of ionizing the molecule in a one-photon process, but the absorption of one dye laser photon and one 5th harmonic photon can ionize the molecule. The net result is that when the dye laser is resonant with a transition, the molecule is carried to the excited state, where absorption of the 5th harmonic radiation leads to efficient ionization. The resulting ions are accelerated in a two-stage Wiley-McLaren ion extraction assembly<sup>57</sup> and travel up a flight tube to a microchannel plate. The output signal is then preamplified (350 MHz) and

digitized for processing in a personal computer. By recording the signal for specific masses of interest as a function of the dye laser wavenumber, the spectra for those species are obtained. After collecting the spectrum of TiFe using the 5th harmonic of the Nd:YAG laser (212.8 nm, 5.83 eV) for ionization, portions of the spectrum were scanned a second time using the 4th harmonic (266 nm, 4.66 eV) for ionization, with the goal of comparing the two scans to place limits on the ionization energy of the TiFe molecule.

To reveal the rotational structure of the observed vibronic bands, the dye laser was scanned in high resolution mode (dual grating,  $0.05 \text{ cm}^{-1}$  resolution) over the various members of the two band systems that were identified. At the same time, a portion of the dye laser output radiation was sent through a cell containing gaseous  $\text{I}_2$ ; another portion was sent through a  $0.22 \text{ cm}^{-1}$  free spectral range étalon. The transmitted intensities were recorded and were used to provide an absolute calibration of the spectrum using the precisely known wavenumbers of the iodine lines that are listed in the  $\text{I}_2$  atlas of Gerstenkorn and Luc.<sup>58</sup> Because in our instrument the TiFe molecules travel at the beam velocity of helium ( $1.77 \times 10^5 \text{ cm/s}$ ) (Ref. 59) toward the dye laser, a small correction for the Doppler shift experienced by the molecules was required. At the same time, a correction for the error in the  $\text{I}_2$  atlas ( $-0.0056 \text{ cm}^{-1}$ ) was also made.<sup>60</sup> Together, these corrections amounted to less than  $0.11 \text{ cm}^{-1}$  for all of the bands reported here.

For a few of the rotationally resolved bands, excited state lifetimes were measured. To do so, the ionization laser was fired at the time of greatest TiFe signal intensity, and the dye laser was scanned in time. The measured ion signal as a function of delay time was then fitted to an exponential decay curve using the Marquardt nonlinear least-squares algorithm.<sup>61</sup>

## III. COMPUTATIONAL DETAILS

For both atoms, Ti and Fe, the correlation consistent basis set of Balabanov and Peterson,<sup>62</sup> 22s18p11d3f2g1h of quadruple cardinality, was employed, generally contracted to [8s7p5d3f2g1h], containing a total of  $104 \times 2 = 208$  spherical Gaussian functions.

The zeroth order wavefunction is of the complete active space self consistent field (CASSCF) type, constructed by allotting the 12 outer electrons ( $4s^2 3d^2/_{\text{Ti}} 4s^2 3d^6/_{\text{Fe}}$ ) to a total of 12 orbitals corresponding to the  $(4s + 3d) \times 2$  atomic orbitals of the two atoms. Under  $C_{2v}$  constraints and depending on the symmetry of the states examined, the above scheme generates  $\sim(55\text{--}95) \times 10^3$  configuration functions (CF). Single and double replacements out of the CASSCF wavefunction give rise to multireference configuration interaction expansions (CASSCF + 1 + 2 = MRCI) of order  $(1.8\text{--}3.5) \times 10^9$  CFs, reduced to  $(1.8\text{--}3.1) \times 10^6$  CFs through the internally contracted approximation.<sup>63,64</sup> The size non-extensivity error at the MRCI(+Q) level, where +Q is the Davidson correction,<sup>65,66</sup> is estimated to be  $\sim 9$  (7.8) mE<sub>h</sub>. We have constructed state averaged potential energy curves (PEC) for  $10^{2S+1}\Lambda$  states, that is  $^1\Sigma^+$ ,  $^1,3\Sigma^-$ ,  $^3\Pi$ ,  $^1\Delta$ ,  $^3\Delta[2]$ ,  $^3\Phi$ , and  $^1,3\Gamma$ , reporting molecular constants extracted through the Dunham

method. Both diagonal and off-diagonal spin-orbit (SO) coupling effects are omitted from these calculations; the first-order spin-orbit splitting of the  $^3\Pi$  state is subsequently computed for comparison to the measured value, however.

All calculations have been performed by the MOLPRO 2010.1 package.<sup>67</sup>

## IV. EXPERIMENTAL RESULTS

### A. Low resolution spectrum

The present spectroscopic study of TiFe covers the range from 15 500  $\text{cm}^{-1}$  to 23 500  $\text{cm}^{-1}$ . This range can be divided into three sections that display qualitatively different spectra. The low energy region, 15 500–19 500  $\text{cm}^{-1}$ , contains only two extremely weak, partially overlapping band systems; the mid-energy region, 19 500–21 500  $\text{cm}^{-1}$ , contains a large number of intense bands, and the high energy region, 21 500–23 500  $\text{cm}^{-1}$ , contains a high density of somewhat weaker transitions. This is illustrated in Figure 1, which displays the low resolution spectrum for the most abundant isotopomer,  $^{48}\text{Ti}^{56}\text{Fe}$  (67.7% natural abundance), over the 16 000–21 500  $\text{cm}^{-1}$  range. Spectra for all of the isotopomers that are present in greater than 1% natural abundance were recorded over the entire scanned range. These include  $^{48}\text{Ti}^{54}\text{Fe}$  (4.3%),  $^{46}\text{Ti}^{56}\text{Fe}$  (7.3%),  $^{47}\text{Ti}^{56}\text{Fe}$  (6.7%),  $^{48}\text{Ti}^{56}\text{Fe}$  (67.7%),  $^{49}\text{Ti}^{56}\text{Fe}$  (5.0%),  $^{48}\text{Ti}^{57}\text{Fe}$  (1.6%), and  $^{50}\text{Ti}^{56}\text{Fe}$  (5.0%). Vibronically and rotationally resolved spectra, tables of line assignments, and fitted spectroscopic constants are available through the supplementary material<sup>68</sup> or from the author (M.D.M.).

The low resolution spectrum of TiFe is remarkably similar to the spectrum of the isovalent molecule, ZrFe, which was recently investigated in our group.<sup>56</sup> Both species have extremely weak vibronic progressions in the 16 000–19 000  $\text{cm}^{-1}$  range (14 000–17 500  $\text{cm}^{-1}$  in ZrFe), fol-

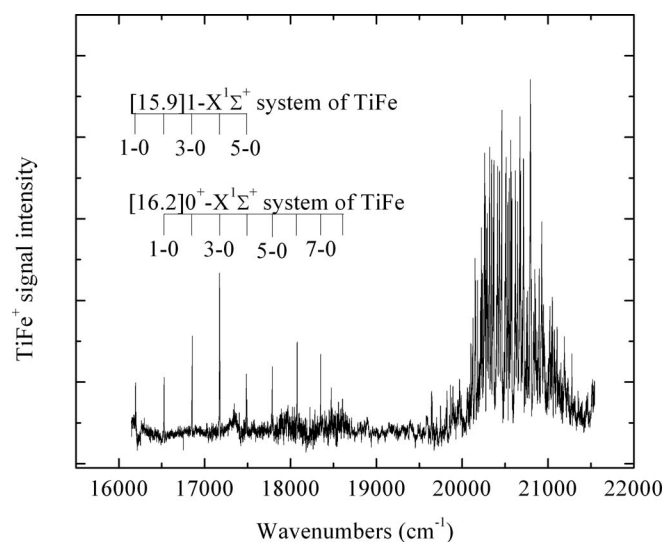


FIG. 1. Low resolution spectrum of diatomic  $^{48}\text{Ti}^{56}\text{Fe}$  over the 16 000–21 500  $\text{cm}^{-1}$  region. The lower energy region, 16 000–19 500  $\text{cm}^{-1}$ , displays what appears to be a single progression, which under higher resolution is revealed to be two partially overlapping progressions. The higher energy region, 19 500–21 500  $\text{cm}^{-1}$ , displays a high density of much stronger transitions.

lowed by a highly congested region of intense transitions at higher energies. For both molecules, high dye laser fluences (8–30  $\text{mJ}/\text{cm}^2$ ) were used for rotational studies of the band systems, and no power broadening was observed. Similarly, the lifetimes of the upper states of the weak band system were found to lie in the range of 14–31  $\mu\text{s}$  for ZrFe, while our studies of the 18 072 and 18 346  $\text{cm}^{-1}$  bands of  $^{48}\text{Ti}^{56}\text{Fe}$  reveal excited state lifetimes of  $23 \pm 4$  and  $26 \pm 6$   $\mu\text{s}$ . The long excited state lifetimes and the lack of power broadening in these spectra demonstrate that the transitions are very weak indeed. Although the weakness of the transitions could result from poor Franck-Condon factors, this would not cause such long excited state lifetimes. Thus, these observations provide strong evidence that the bands correspond to spin-forbidden transitions, a possibility that is further supported by computational studies that are reported below. The observation of strong transitions above 20 000  $\text{cm}^{-1}$  also suggests that the upper states of the spin-forbidden transitions borrow intensity from these higher-lying, strongly allowed states by mixing that is induced by spin-orbit interactions. In this context, we note that the orbital spin-orbit parameters are given by  $\zeta_{3d}(\text{Ti}) = 123$   $\text{cm}^{-1}$  and  $\zeta_{3d}(\text{Fe}) = 417$   $\text{cm}^{-1}$ .<sup>69</sup> These values are large enough to allow admixtures of a few percent of the strongly allowed character into the spin-forbidden states, consistent with the long lifetimes and low susceptibility to power broadening that are observed.

Following the initial survey of the spectrum that was undertaken using the fifth harmonic of the Nd:YAG laser (212.8 nm) for ionization, portions of the spectrum were rescanned using the fourth harmonic, 266 nm, for ionization in order to bracket the ionization energy of the molecule. The lowest energy transition that could be observed with the 266 nm (4.661 eV) radiation lies at 20 178  $\text{cm}^{-1}$  (2.502 eV), placing the ionization energy below 7.16 eV. It was found that the 5-0 band of the  $[16.2]0^+ \leftarrow X^1\Sigma^+$  system, which lies at 17 788  $\text{cm}^{-1}$  (2.205 eV) could not be observed using 266 nm radiation for ionization, thereby placing the ionization energy of TiFe above 6.86 eV. On this basis, the ionization energy of TiFe is thought to lie in the range  $6.86$  eV  $< \text{IE}(\text{TiFe}) < 7.16$  eV. This is similar to the ionization energy of the isoelectronic molecule,  $\text{Cr}_2$ , which has been established as 6.999(1) eV.<sup>70</sup>

In a large number of diatomic transition metals, predissociation is found to set in abruptly as soon as the energy exceeds the energy of the lowest separated atom limit, particularly when a large density of electronic states is present.<sup>71–76</sup> Given the large density of states evident toward higher energies in Figure 1, scans were conducted to higher wavenumbers in the hope of finding a predissociation threshold. Despite scanning slightly beyond 23 500  $\text{cm}^{-1}$ , no predissociation threshold was found. On this basis, we believe that the bond energy of TiFe is greater than the wavenumber of the last observed band, placing  $D_0(\text{TiFe})$  above 2.91 eV.

A vibrational progression consisting of eight bands was found in the survey scan over the 16 000–19 000  $\text{cm}^{-1}$  region. Higher resolution (0.05  $\text{cm}^{-1}$ ) studies, however, revealed that four members of the apparent progression consisted of two closely spaced bands of different upper state electronic symmetry. One band had P, Q, and R branches, with first lines of



R(0), Q(1), and P(2); the second band displayed only P and R branches, with first lines of R(0) and P(1). Accordingly, what was on first glance only a single band system was instead assigned to two systems that were eventually labeled as the  $[15.9]1 \leftarrow X^1\Sigma^+$  and  $[16.2]0^+ \leftarrow X^1\Sigma^+$  systems. The detailed rotational analysis and the reasoning behind this assignment are presented below.

For all of the bands belonging to the two band systems, rotationally resolved spectra were collected and analyzed, allowing band origins and isotope shifts to be precisely measured. These values were then used to establish the vibrational numbering of the bands. By assuming a vibrational numbering and fitting the band origins of the heavier isotopomer to the standard formula,<sup>77</sup>

$$\nu = T_0 + \nu'\omega'_e - (\nu'^2 + \nu')\omega'_e x'_e, \quad (1)$$

the fitted spectroscopic constants  $\omega'_e$  and  $\omega'_e x'_e$  could be used to calculate the predicted isotope shift using the formula<sup>77</sup>

$$\begin{aligned} \nu_L - \nu_H = & (\rho - 1)[\omega'_e(\nu' + 1/2) - \omega''_e(1/2)] \\ & - (\rho^2 - 1)[\omega'_e x'_e(\nu' + 1/2)^2 - \omega''_e x''_e(1/2)^2]. \end{aligned} \quad (2)$$

For TiFe, the heavy isotopomer ( $\nu_H$ ) was chosen to be  $^{50}\text{Ti}^{56}\text{Fe}$  because of the lack of other observable isotopic combinations at mass 106. The light isotopomer ( $\nu_L$ ) was chosen as  $^{48}\text{Ti}^{56}\text{Fe}$  due to its high abundance, combined with the lack of other observable isotopomers at mass 104. For these species, the dimensionless parameter,  $\rho$ , is given as  $\rho = \sqrt{\frac{\mu_H}{\mu_L}} = 1.01670$ . By treating Eqs. (1) and (2) as functions of a continuous parameter,  $\nu'$ , it was possible to plot the predicted isotope shift,  $\nu(^{48}\text{Ti}^{56}\text{Fe}) - \nu(^{50}\text{Ti}^{56}\text{Fe})$ , as a function of the band frequency,  $\nu$ , for various assignments of the bands. The resulting curves were then compared to the measured isotope shift and band origin values to identify the correct vibrational numbering. To do so, the ground state vibrational frequency,  $\omega_e''$  was taken from the computations reported below as  $534\text{ cm}^{-1}$  and the anharmonicity,  $\omega_e'' x_e''$  was neglected, as its effect on the isotope shift is minimal.

The resulting plots are unequivocal. Figure 2 shows the isotope shift vs. transition wavenumber plot for the  $[15.9]1 \leftarrow X^1\Sigma^+$  band system, which establishes that the first observed band, found near  $16\,191\text{ cm}^{-1}$  in  $^{48}\text{Ti}^{56}\text{Fe}$ , is the 1-0 band. Likewise, Figure 3 demonstrates that the first observed band of the  $[16.2]0^+ \leftarrow X^1\Sigma^+$  system, found near  $16\,525\text{ cm}^{-1}$  in  $^{48}\text{Ti}^{56}\text{Fe}$ , is also the 1-0 band.

Fitting all vibronic bands that belong to the same band system to Eq. (1), then gives the values of  $T_0$ ,  $\omega'_e$ , and  $\omega'_e x'_e$  for the various isotopomers. The resulting fitted vibrational constants for the  $[15.9]1 \leftarrow X^1\Sigma^+$  and  $[16.2]0^+ \leftarrow X^1\Sigma^+$  band systems are presented in Table I.

## B. Rotationally resolved spectra

All of the bands that were found in survey scans ( $0.14\text{ cm}^{-1}$  resolution) in the  $16\,000\text{--}19\,000\text{ cm}^{-1}$  region were subsequently investigated in high resolution ( $0.05\text{ cm}^{-1}$ ). At this higher resolution, four features, located

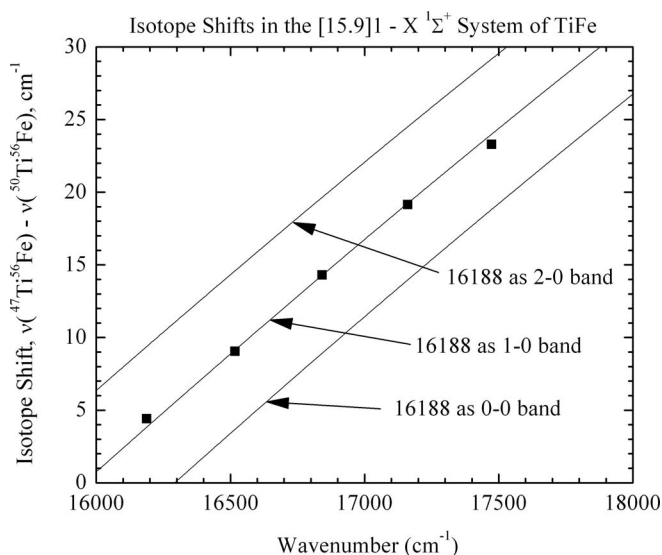


FIG. 2. Determination of the vibrational assignment for the  $[15.9]^3\Pi_1 \leftarrow ^1\Sigma^+$  band system. Solid lines provide the calculated isotope shift, plotted against the band origin wavenumber for three different assignments. The measured isotope shifts are plotted as black squares and are in excellent agreement with the calculated shifts, when the  $16\,188\text{ cm}^{-1}$  band is assigned as the 1-0 band.

near  $16\,525$ ,  $16\,849$ ,  $17\,168$ , and  $17\,480\text{ cm}^{-1}$ , were found to consist of two bands within a few  $\text{cm}^{-1}$  of each other. This is illustrated in Figure 4, which displays the rotationally resolved spectrum near  $17\,480\text{ cm}^{-1}$  for the most abundant isotopomer,  $^{48}\text{Ti}^{56}\text{Fe}$ . Above  $17\,480\text{ cm}^{-1}$ , the observed features consisted of only a single band, as displayed in Figure 5. All of the features that were found to contain pairs of bands were similar to that shown in Figure 4, with both bands red shaded, displaying R branch band heads at low values of  $J$  and a series of P lines marching off to lower wavenumbers. In fact, all of

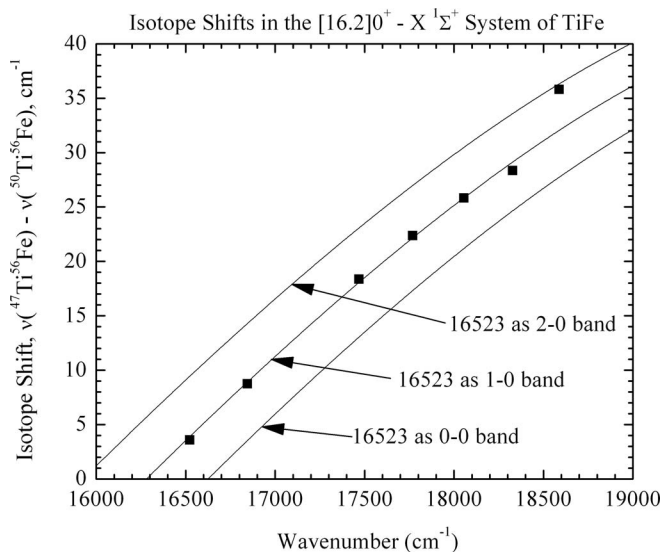


FIG. 3. Determination of the vibrational assignment for the  $[16.2]^3\Pi_0^+ \leftarrow ^1\Sigma^+$  band system. Solid curves provide the calculated isotope shift, plotted against the band origin wavenumber for three different assignments. The measured isotope shifts are plotted as black squares and are in excellent agreement with the calculated shifts, when the  $16\,523\text{ cm}^{-1}$  band is assigned as the 1-0 band.

TABLE I. Results from a vibronic fit of bands belonging to the  $[15.9]^3\Pi_1 \leftarrow X^1\Sigma^+$  and the  $[16.2]^3\Pi_0^+ \leftarrow X^1\Sigma^+$  band systems of TiFe.

	$^{46}\text{Ti}^{56}\text{Fe}$	$^{48}\text{Ti}^{54}\text{Fe}$	$^{47}\text{Ti}^{56}\text{Fe}$	$^{48}\text{Ti}^{56}\text{Fe}$	$^{49}\text{Ti}^{56}\text{Fe}$	$^{50}\text{Ti}^{56}\text{Fe}$
Fitted spectroscopic constants for the $[15.9]^3\Pi_1 \leftarrow X^1\Sigma^+$ band system <sup>a</sup>						
$T_0$ (cm <sup>-1</sup> )	15 849.67(64)		15 851.54(89)	15 851.95(84)	15 852.39(51)	15 852.54(32)
$\omega_e'$ (cm <sup>-1</sup> )	349.175(589)		346.156(784)	344.309(741)	342.471(459)	340.683(287)
$\omega_e'x_e'$ (cm <sup>-1</sup> )	3.000(85)		2.841(110)	2.822(104)	2.808(63)	2.743(40)
$k_e'$ (mdyn/Å)	1.812		1.802	1.803	1.804	1.804
Fitted spectroscopic constants for the $[16.2]^3\Pi_0^+ \leftarrow X^1\Sigma^+$ band system						
$T_0$ (cm <sup>-1</sup> )	16 179.51(461)	16 182.00(522)	16 180.71(442)	16 183.42(502)	16 180.41(500)	16 181.54(476)
$\omega_e'$ (cm <sup>-1</sup> )	355.99(260)	352.98(3351)	353.39(249)	349.51(322)	351.59(288)	349.20(274)
$\omega_e'x_e'$ (cm <sup>-1</sup> )	5.443(255)	5.170(366)	5.315(244)	5.021(352)	5.466(286)	5.347(272)
$k_e'$ (mdyn/Å)	1.884	1.895	1.874	1.900	1.879	1.922

<sup>a</sup>Error limits (1 $\sigma$ ) for the resulting fitted spectroscopic constants are provided in units of the last digit quoted.

the observed bands, even those which appeared as single features, were red shaded, indicating an increase in bond length upon electronic excitation.

For the features that turned out to consist of pairs of bands, one of the bands had only R and P branches with first lines of R(0) and P(1) while the second band had R, Q, and P branches with first lines of R(0), Q(1), and P(2). These first lines demonstrate that the  $\Omega$  values for the band systems are  $\Omega' = 0 \leftarrow \Omega'' = 0$  for the bands containing only R and P lines, and  $\Omega' = 1 \leftarrow \Omega'' = 0$  for the bands with all three branches. Further analysis demonstrated that all of the bands originate from the same lower state. Accordingly, the bands were fitted to the standard form

$$\nu(J' \leftarrow J'') = \nu_0 + B'J'(J' + 1) - B''J''(J'' + 1), \quad (3)$$

with  $B''$  constrained to be the same for all bands belonging to the same isotopomer. This procedure provides the most accurate values of  $B''$  and the various  $B_v'$  values as well. For the most abundant  $^{48}\text{Ti}^{56}\text{Fe}$  isotopomer the values of  $B''$  and  $r_0''$  were found to be 0.225 228(31) cm<sup>-1</sup> and 1.702 68(12) Å respectively (1 $\sigma$  error limits given in parentheses). Fitted ground state molecular constants for the remaining TiFe isotopomers are presented in Table II. Combining the results for all of the masses for which only a single iso-

topomer was observed ( $^{47}\text{Ti}^{56}\text{Fe}$ ,  $^{48}\text{Ti}^{56}\text{Fe}$ , and  $^{50}\text{Ti}^{56}\text{Fe}$ ), we obtain our best estimate of the ground state bond length as  $r_0'' = 1.7024(3)$  Å.

This bond length is similar to that of the isoelectronic Cr<sub>2</sub> molecule ( $r_0'' = 1.6858$  Å),<sup>8</sup> suggesting that the  $\Omega = 0$  ground state of TiFe is also a closed-shell,  $^1\Sigma^+$  state. This is supported by a density functional calculation that provides a calculated bond length of 1.67 Å for the predicted  $^1\Sigma^+$  ground state<sup>55</sup> and by *ab initio* calculations reported below. Based on the good agreement between theory and experiment, we assign the ground state as  $X^1\Sigma^+$ . This implies that the upper state of the  $[16.2]0$  system has  $\Omega = 0^+$ , since transitions from a  $^1\Sigma^+(\Omega = 0^+)$  state to a state with  $\Omega = 0^-$  are strictly forbidden in the absence of heterogeneous perturbations.

Excluding bands that were obviously perturbed, the fitted values of  $B_v'$  for the bands belonging to  $[15.9]1 \leftarrow X^1\Sigma^+$  and  $[16.2]0^+ \leftarrow X^1\Sigma^+$  band systems were fitted to the expression,

$$B_v' = B_e' - \alpha_e'(v + 1/2), \quad (4)$$

to determine the constants  $B_e'$  and  $\alpha_e'$  for these two band systems. Values of  $B_v'$ ,  $B_e'$ ,  $r_e'$ , and  $\alpha_e'$  for the different isotopic modifications of TiFe are presented in Table III. In the table,

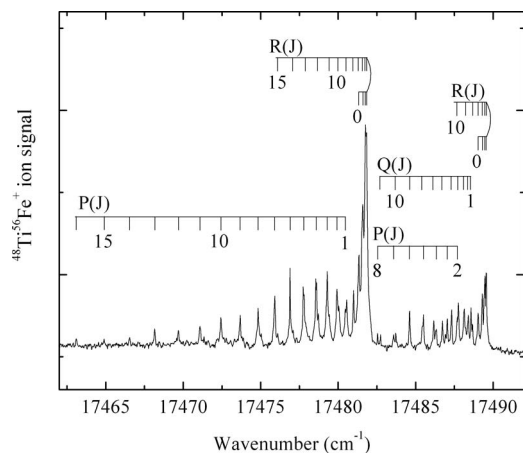


FIG. 4. Rotationally resolved spectrum of the 5-0 band of the  $[15.9]^3\Pi_1-X^1\Sigma^+$  system (on the right), and the 4-0 band of the  $[16.2]^3\Pi_0^+-X^1\Sigma^+$  system (on the left).

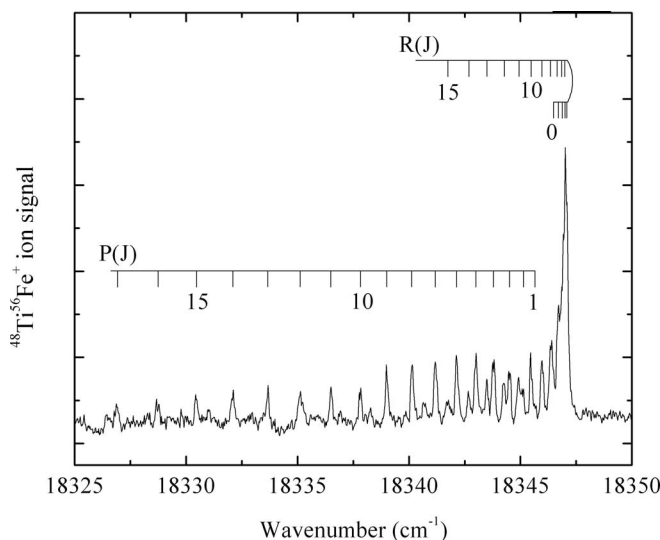


FIG. 5. Rotationally resolved spectrum of the 7-0 band of the  $[16.2]^3\Pi_0^+-X^1\Sigma^+$  system.

TABLE II. Fitted ground state rotational constants and bond length for TiFe isotopomers obtained in a combined fit of all rotationally resolved bands.<sup>a</sup>

	<sup>46</sup> Ti <sup>56</sup> Fe	<sup>48</sup> Ti <sup>54</sup> Fe	<sup>47</sup> Ti <sup>56</sup> Fe	<sup>48</sup> Ti <sup>56</sup> Fe	<sup>49</sup> Ti <sup>56</sup> Fe	<sup>50</sup> Ti <sup>56</sup> Fe
B <sub>0</sub> <sup>''</sup> (cm <sup>-1</sup> )	0.230619(56)	0.229557(86)	0.227903(41)	0.225228(31)	0.222829(51)	0.220525(56)
r <sub>0</sub> <sup>''</sup> (Å)	1.70222(21)	1.70088(32)	1.70230(15)	1.70268(12)	1.70238(19)	1.70212(22)

<sup>a</sup>Errors (1σ) are provided for all fitted spectroscopic constants in parentheses following the reported value, in units of the last digit quoted.

the value of  $\alpha_e$  calculated from the Pekeris relationship,<sup>78</sup>

$$\alpha_e = [6(\omega_e x_e B_e^3)^{1/2} - 6B_e^2]/\omega_e, \quad (5)$$

is also provided. The Pekeris values of  $\alpha_e$  are in poor agreement with the fitted results, providing additional evidence that the observed states are perturbed, either by  $\Delta\Omega = 0$  spin-orbit mixing with another state or via  $\Delta\Omega = 1$  L-uncoupling interactions with another state. Inverting the values of  $B_e'$  to obtain  $r_e'$ , and combining the results for the masses having only a single observable isotopomer, we obtain our best estimates of the equilibrium bond lengths of the upper states as  $r_e'([15.9]1) = 1.8857(36)$  Å and  $r_e'([16.2]0^+) = 1.8839(22)$  Å.

### C. The nature of the [15.9]1 and [16.2]0<sup>+</sup> excited states

The similar bond lengths in the [15.9]1 and [16.2]0<sup>+</sup> states, along with the similar vibrational frequencies of

344.3(7) and 349.5(3.2) cm<sup>-1</sup>, respectively, suggest that the two states may be spin-orbit components of the same Hund's case (a) state. If so, the Hund's case (a) state must be inverted, with the bottom of the  $\Omega = 1$  well lying about 329.4 cm<sup>-1</sup> below the bottom of the  $\Omega = 0^+$  well.

The weak intensity of the observed band systems suggests that they are electronically forbidden, presumably gaining intensity through spin-orbit mixing with the intense upper states that lie further to the blue. Although the Hund's case (a) state responsible for both the [15.9]1 and [16.2]0<sup>+</sup> states could be either a  $^3\Sigma^-$  or a  $^3\Pi$  state, a  $^3\Sigma^-$  state would undergo spin-orbit splitting only in the second order of perturbation theory, leading to a small splitting. Also, some departure from the  $B'/J'(J' + 1)$  formula would be expected at higher J values, due to spin-uncoupling interactions between the  $^3\Sigma^-(0^+)$  and  $^3\Sigma^-(1)$  components. Thus, it is likely that the observed [15.9]1 and [16.2]0<sup>+</sup> states are components of an inverted  $^3\Pi$  state.

TABLE III. Results from the fits of bands belonging to [15.9]<sup>3</sup>Π<sub>1</sub> and [16.2]<sup>3</sup>Π<sub>0</sub><sup>+</sup> states of TiFe.<sup>a</sup>

Vibrational level	B <sub>v</sub> <sup>'</sup> ( <sup>46</sup> Ti <sup>56</sup> Fe)	B <sub>v</sub> <sup>'</sup> ( <sup>48</sup> Ti <sup>54</sup> Fe)	B <sub>v</sub> <sup>'</sup> ( <sup>47</sup> Ti <sup>56</sup> Fe)	B <sub>v</sub> <sup>'</sup> ( <sup>48</sup> Ti <sup>56</sup> Fe)	B <sub>v</sub> <sup>'</sup> ( <sup>49</sup> Ti <sup>56</sup> Fe)	B <sub>v</sub> <sup>'</sup> ( <sup>50</sup> Ti <sup>56</sup> Fe)
[15.9] <sup>3</sup> Π <sub>1</sub> state of TiFe						
1	0.18772(21)		0.18399(−38)	0.18248(−5)	0.18246(−1)	0.17496 <sup>b</sup>
2			0.18436(50)	0.18214(20)	0.18026(1)	0.178323(20)
3	0.18549(−32)		0.18352(17)	0.18125(−10)	0.17801(−1)	0.177405(−41)
4	0.18474(−21)		0.18255(−30)	0.18056(−20)		0.176610(20)
5	0.18442(32)		0.18236(2)	0.18033(15)	0.17816 <sup>b</sup>	0.17917 <sup>b</sup>
Fitted spectroscopic constants for the [15.9] <sup>3</sup> Π <sub>1</sub> state of TiFe						
B <sub>e</sub> <sup>'</sup> (cm <sup>-1</sup> )	0.18878(58)		0.18513(55)	0.18341(26)	0.18581(3)	0.18044(14)
r <sub>e</sub> <sup>'</sup> (Å)	1.8970(29)		1.8887(28)	1.8868(13)	1.8643(2)	1.8817(7)
α <sub>e</sub> <sup>'</sup> (cm <sup>-1</sup> )	0.000850(282)		0.000508(276)	0.000589(132)	0.002226(18)	0.000856(75)
α <sub>e</sub> <sup>'</sup> (Pekeris) <sup>c</sup>	0.001829		0.001733	0.001713	0.001747	0.001662
[16.2] <sup>3</sup> Π <sub>0</sub> <sup>+</sup> state of TiFe						
1	0.18716(9)	0.18615(0)	0.18499(0)	0.18261(−9)	0.18078(9)	0.17885(6)
2	0.18630(−10)	0.18533(0)	0.18412(−2)	0.18183(18)	0.17998(−14)	0.17819(−10)
3	0.18569(−6)	0.18451(0)	0.18329(1)	0.18050(−9)		
4	0.18516(8)	0.18453 <sup>b</sup>	0.18309 <sup>b</sup>	0.18108 <sup>b</sup>	0.17901(4)	0.17732(3)
5	0.18588 <sup>b</sup>	0.18439 <sup>b</sup>	0.18364 <sup>b</sup>	0.18144 <sup>b</sup>	0.17948 <sup>b</sup>	0.17756 <sup>b</sup>
6	0.18702 <sup>b</sup>	0.18701 <sup>b</sup>	0.18481 <sup>b</sup>	0.18254 <sup>b</sup>	0.18051 <sup>b</sup>	0.17862 <sup>b</sup>
7	0.18354 <sup>b</sup>	0.18488 <sup>b</sup>	0.18417 <sup>b</sup>	0.18283 <sup>b</sup>	0.18162 <sup>b</sup>	0.17967 <sup>b</sup>
8	0.18715 <sup>b</sup>		0.18120 <sup>b</sup>		0.17624 <sup>b</sup>	0.17841 <sup>b</sup>
Fitted spectroscopic constants for the [16.2] <sup>3</sup> Π <sub>0</sub> <sup>+</sup> state of TiFe						
B <sub>e</sub> <sup>'</sup> (cm <sup>-1</sup> )	0.18806(20)	0.18739(0)	0.18625(4)	0.18429(48)	0.18155(28)	0.17954(19)
r <sub>e</sub> <sup>'</sup> (Å)	1.8850(2)	1.8826(0)	1.8831(2)	1.8823(25)	1.8860(15)	1.8864(10)
α <sub>e</sub> <sup>'</sup> (cm <sup>-1</sup> )	0.000660(107)	0.000822(4)	0.000847(27)	0.001056(292)	0.000576(154)	0.000499(108)
α <sub>e</sub> <sup>'</sup> (Pekeris) <sup>c</sup>	0.002611	0.002538	0.002560	0.002433	0.002539	0.002452

<sup>a</sup>Residuals in the fit of the B<sub>v</sub><sup>'</sup> values are provided in parentheses following each entry, in units of 0.00001 cm<sup>-1</sup>. Error limits (1σ) for the resulting fitted spectroscopic constants are provided in units of the last digit quoted.<sup>b</sup>Omitted from the fit, because the B<sub>v</sub><sup>'</sup> value showed evidence of perturbations, specifically, a failure of the B<sub>v</sub><sup>'</sup> values to decrease with increasing v<sup>'</sup>.<sup>c</sup>The value of α<sub>e</sub> calculated from the Pekeris relationship, α<sub>e</sub> = [6(ω<sub>e</sub>x<sub>e</sub>B<sub>e</sub><sup>3</sup>)<sup>1/2</sup> − 6B<sub>e</sub><sup>2</sup>]/ω<sub>e</sub>, should be close to the fitted value if the bands are unperturbed and follow a Morse potential reasonably closely. The failure of the calculated values to match the fitted values shows that the levels are either perturbed or follow a potential that differs significantly from the Morse potential.

Given that the leading contribution to the  $^1\Sigma^+$  ground state is a  $1\sigma^2 2\sigma^2 1\pi^4 1\delta^4$  configuration (see below),  $^3\Pi$  states can be generated by one-electron promotions of a  $1\sigma$  or  $2\sigma$  electron to the  $2\pi$  orbital, a  $1\delta$  electron to the  $2\pi$  orbital, a  $1\pi$  electron to the  $2\delta$  orbital, or a  $1\pi$  electron to the  $3\sigma$  or  $4\sigma$  orbital. In terms of the partially occupied orbitals, these lead to  $1\sigma^1 2\pi^1$ ,  $2\sigma^1 2\pi^1$ ,  $1\delta^3 2\pi^1$ ,  $1\pi^3 2\delta^1$ ,  $1\pi^3 3\sigma^1$  and  $1\pi^3 4\sigma^1$  configurations. The first of these,  $1\sigma^1 2\pi^1$  or  $2\sigma^1 2\pi^1$ , has the orbital that is responsible for the spin-orbit splitting ( $2\pi$ ) less than half-full, so the resulting  $^3\Pi$  state would be regular, not inverted. These configurations may be excluded from further consideration. The last two configurations move an electron from a strongly bonding  $1\pi$  orbital to a strongly antibonding  $3\sigma$  or  $4\sigma$  orbital, and would not be expected to arise at such a low energy. The remaining two configurations,  $1\delta^3 2\pi^1$  and  $1\pi^3 2\delta^1$ , have an orbital that is more than half-full (favoring an inverted  $^3\Pi$  state) and another orbital that is less than half-full (favoring a regular  $^3\Pi$  state). Thus, more detailed consideration is required to decide which of these could be consistent with the data.

To consider the spin-orbit splitting expected for the  $1\delta^3 2\pi^1$ ,  $^3\Pi$  and  $1\pi^3 2\delta^1$ ,  $^3\Pi$  states, we note that the spin-orbit operator can be expressed as an effective one-electron operator given by<sup>69,79</sup>

$$\hat{H}^{\text{SO}} = \sum_{i\alpha} \hat{a}_{i\alpha} \hat{\ell}_{i\alpha} \cdot \hat{s}_i, \quad (6)$$

where the sum is over all electrons,  $i$ , and nuclei,  $\alpha$ . Here  $\hat{a}_{i\alpha}$  is an operator that depends only on the distance of electron  $i$  from nucleus  $\alpha$ ,  $r_{i\alpha}$ ;  $\hat{\ell}_{i\alpha}$  is the orbital angular momentum operator for electron  $i$  measured about nucleus  $\alpha$ ; and  $\hat{s}_i$  is the spin angular momentum operator of electron  $i$ . In the first-order perturbation treatment of the spin-orbit interaction of a  $^3\Pi$  state, the spin-orbit energy is given by  $E^{\text{SO}} = A\Lambda\Sigma$ , where  $\Lambda$  and  $\Sigma$  are the projections of  $L$  and  $S$  on the internuclear axis, respectively, and  $A$  is the spin-orbit constant for the state in question. As a result,  $E^{\text{SO}}$  vanishes for a  $^3\Pi_1$  state ( $\Lambda = 1$ ,  $\Sigma = 0$ ), but the  $^3\Pi_0$  component ( $\Lambda = 1$ ,  $\Sigma = -1$ ) has a nonzero spin-orbit energy ( $-A$ ) given by

$$E^{\text{SO}}(^3\Pi_0) = -A = \langle ^3\Pi_0 | \hat{H}^{\text{SO}} | ^3\Pi_0 \rangle. \quad (7)$$

Treating the  $^3\Pi_0$  states as single Slater determinants, and applying the Slater-Condon rules for the evaluation of one-electron operators,<sup>80</sup> it is possible to express the spin-orbit energies in terms of the parameters  $a_\delta \equiv \langle \delta | \sum_\alpha \hat{a}_\alpha | \delta \rangle$  and  $a_\pi \equiv \langle \pi | \sum_\alpha \hat{a}_\alpha | \pi \rangle$  as<sup>69</sup>

$$E^{\text{SO}}(1\delta^3 2\pi^1, ^3\Pi_0) = a_\delta + \frac{1}{2}a_\pi \quad (8)$$

and

$$E^{\text{SO}}(1\pi^3 2\delta^1, ^3\Pi_0) = -a_\delta - \frac{1}{2}a_\pi. \quad (9)$$

For a  $\pi$  orbital that is expressed as  $\pi = c_1 3d\pi(\text{Ti}) + c_2 3d\pi(\text{Fe})$ ,  $a_\pi$  is given by

$$a_\pi = |c_1|^2 \zeta_{3d}(\text{Ti}) + |c_2|^2 \zeta_{3d}(\text{Fe}). \quad (10)$$

Similarly, for a  $\delta$  orbital that is expressed as  $\delta = c'_1 3d\delta(\text{Ti}) + c'_2 3d\delta(\text{Fe})$ ,  $a_\delta$  is given by

$$a_\delta = |c'_1|^2 \zeta_{3d}(\text{Ti}) + |c'_2|^2 \zeta_{3d}(\text{Fe}). \quad (11)$$

If we estimate that the  $\pi$  and  $\delta$  orbitals have equal contributions on the two atoms, then we expect  $a_\pi = a_\delta = \frac{1}{2}[\zeta_{3d}(\text{Ti}) + \zeta_{3d}(\text{Fe})] = 270 \text{ cm}^{-1}$ . Thus, Eqs. (8) and (9) predict that the  $1\delta^3 2\pi^1$ ,  $^3\Pi$  state will be inverted, with a  $^3\Pi_0 - ^3\Pi_1$  energy difference of about  $405 \text{ cm}^{-1}$ , while the  $1\pi^3 2\delta^1$ ,  $^3\Pi$  state will be regular, with a  $^3\Pi_0 - ^3\Pi_1$  energy difference of about  $-405 \text{ cm}^{-1}$ . The experimentally measured separation of  $^3\Pi_0 - ^3\Pi_1 = 329.4 \text{ cm}^{-1}$  strongly suggests that the excited state is a  $^3\Pi$  state deriving from a  $1\delta^3 2\pi^1$  configuration. Alternatively, using the calculated molecular orbitals obtained below,  $1\delta \sim (0.30) 3d\delta_{\text{Ti}} + (0.93) 3d\delta_{\text{Fe}}$  and  $2\pi \sim (0.80) 3d\pi_{\text{Ti}} + (0.61) 3d\pi_{\text{Fe}}$ , we obtain a calculated  $^3\Pi_0 - ^3\Pi_1$  energy difference for the  $1\delta^3 2\pi^1$ ,  $^3\Pi$  state of  $489 \text{ cm}^{-1}$ . The difference between the measured spin-orbit splitting ( $329.4 \text{ cm}^{-1}$ ) and that calculated by this method ( $405$  or  $489 \text{ cm}^{-1}$ ) is likely due to second-order spin-orbit effects arising from interactions with other nearby states, which can shift the  $^3\Pi_0$  level relative to the  $^3\Pi_1$  level. Even so, the fact that the  $1\delta^3 2\pi^1$  configuration is the only one that produces an inverted  $^3\Pi$  state provides strong evidence that this assignment is correct. This conclusion is borne out in *ab initio* calculations that are reported below.

## D. Intense transitions in the 20 000–21 500 $\text{cm}^{-1}$ region

In the 20 000–21 500 range, TiFe displays a high density of vibronic transitions that are notable for their high intensity. In this regard, TiFe is reminiscent of the coinage metal dimers,  $\text{Cu}_2$ ,<sup>81</sup>  $\text{CuAg}$ ,<sup>82</sup>  $\text{CuAu}$ ,<sup>83</sup>  $\text{AgAu}$ ,<sup>84</sup> and  $\text{Au}_2$ ,<sup>84</sup> and the group 6 dimers  $\text{CrMo}$  (Ref. 85) and  $\text{Mo}_2$ ,<sup>86</sup> all of which exhibit similarly intense transitions in the blue region ( $19\,300$ – $25\,900 \text{ cm}^{-1}$ ) that have short fluorescence state lifetimes ( $\tau = 14$ – $40 \text{ ns}$ ) and large absorption oscillator strengths ( $f = 0.08$ – $0.24$ ). In the case of the coinage metal dimers, we have previously argued that ion pair states arising from the  $\text{M}^+ + \text{M}^-$  separated ion limit are found in this energy range as a result of the long-range attraction of the ions,<sup>82–84,87</sup> which, ignoring polarization effects, bond formation, and short-range repulsions, have potential energy curves given by

$$V(R) = D_e(M - M', X^1\Sigma^+) + \text{IE}(M) - \text{EA}(M') - 116138 \text{ cm}^{-1}/R(\text{\AA}). \quad (12)$$

In the case of  $\text{Au}_2$ , *ab initio* calculations clearly identify the  $\text{B } 0_u^+$  state ( $\tau = 18 \text{ ns}$ ,  $f = 0.13$ ) (Ref. 84) as correlating diabatically to the  $\text{Au}^+ + \text{Au}^-$  separated ion limit.<sup>88</sup> Further, transitions from the covalent ground state to these ion-pair states are charge transfer transitions that have large transition dipole moments. Thus, for the coinage metal dimers and by extension the group 6 dimers, ion pair states provide a source of considerable oscillator strength that is shared with other states of the appropriate symmetry through state mixing via configuration interaction and spin-orbit interaction.

There is no reason why these ion-pair states should be limited to the coinage metal or group 6 dimers. In fact, this mechanism is expected to provide an important source of oscillator strength in the blue region of the spectrum for all of the transition metal diatomics, owing to the similarity of



TABLE IV. Energies  $E$  ( $E_h$ ), bond lengths  $r_e$  ( $\text{\AA}$ ), dissociation energies  $D_e$  (kcal/mol), harmonic frequencies and anharmonic corrections  $\omega_e$ ,  $\omega_e x_e$  ( $\text{cm}^{-1}$ ), total Mulliken charges on Fe  $q_{\text{Fe}}$ , dipole moments  $\mu$  (Debye), and energy separations  $T_e$  ( $\text{cm}^{-1}$ ) of  $^{48}\text{Ti}^{56}\text{Fe}$  at the MRCI(+Q) level.

State	$-E$	$r_e$	$D_e^a$	$\omega_e$	$\omega_e x_e$	$q_{\text{Fe}}$	$\langle\mu\rangle/\mu_{\text{FF}}^b$	$T_e$
$X^1\Sigma^+{}^c$	2111.176 02 (2111.202 9)	1.707 (1.724)	70.6 (71.3)	560 (534)	2.3 (3.5)	+0.36	1.96/1.74 (1.85)	0.0 (0.0)
$^1\Delta$	2111.126 25 (2111.165 2)	2.096	39.3 (47.6)			+0.22	0.10/	10 923 (8274)
$^3\Delta[1]$	2111.126 22 (2111.169 9)	2.06	39.3 (50.6)	309	2.3	+0.24	0.20/	10 929 (7243)
$^1\Sigma^-$	2111.115 98 (2111.154 0)	1.925	32.9 (40.6)	310	0.40	+0.31	1.09/	13 178 (10 732)
$^1\Gamma$	2111.114 68 (2111.157 5)	1.933	32.1 (42.8)	323	0.18	+0.31	1.04/	13 463 (9964)
$^3\Gamma$	2111.111 50 (2111.150 1)	1.871	30.1 (38.1)			+0.31	1.34/	14 161 (11 588)
$^3\Sigma^-$	2111.110 49 (2111.149 8)	1.877	29.4 (38.0)			+0.31	1.28/	14 382 (11 654)
$^3\Delta[2]$	2111.104 50 (2111.155 8)	2.160	25.7 (41.7)	319	2.40	+0.22	0.22/	15 697 (12 817)
$^3\Phi, ^3\Pi^d$	2111.081 0 (2111.124 6)	1.846	11 (22.1)			+0.44	2.14/	20 854 (17 185)

<sup>a</sup>With respect to  $\text{Ti}(4s^1 3d^3; a^5D) + \text{Fe}(4s^2 3d^6; a^5D)$ .

<sup>b</sup> $\langle\mu\rangle$  calculated as expectation value,  $\mu_{\text{FF}}$  by the finite-field method; field strength ranges from  $10^{-6}$  to  $10^{-5}$  a.u.

<sup>c</sup>State specific calculation.

<sup>d</sup>Degenerate pair.

ionization energies and electron affinities for these species. In the case of TiFe, if we estimate the bond energy to be 3 eV (see below) and employ  $\text{IE}(\text{Ti}) = 6.828$  eV (Ref. 89) and  $\text{EA}(\text{Fe}) = 0.163$  eV,<sup>90</sup> Eq. (12) predicts that the lowest ion pair states should lie in the vicinity of  $20\,000\text{ cm}^{-1}$  at  $R = 2.0\text{ \AA}$ , quite close to the energy where intense transitions begin. The same mechanism has been invoked to explain the intense transitions in ZrFe that occur in a similar spectral region.<sup>56</sup>

## V. COMPUTATIONAL STUDIES

### A. The nature of the beast

Our previous theoretical work on the homonuclear 3d metal diatomics,  $\text{Sc}_2$ ,<sup>91</sup>  $\text{Ti}_2$ ,<sup>92</sup> and  $\text{Mn}_2$ ,<sup>93</sup> showed most clearly the very many difficulties with which one is confronted, even for obtaining “reliable qualitative” results. At first this is surprising, considering that we are dealing with a relatively small number of active (outer) electrons, 12, and just two nuclei that are not very heavy, making it a rather chemically trivial system. However, the very large density of the 3d–M atomic states of high orbital and spin angular momenta, the rather unfavorable atomic configurations for bond formation, and the intense multireference nature of the 3d– $\text{M}_2$  molecules provide poor conditions for accurate all–electron *ab initio* calculations. Our experimental and theoretical results (*vide infra*) indicate that the ground state of TiFe is of  $^1\Sigma^+$  symmetry, with the *in situ* atoms in the  $a^5F(4s^1 3d^3)$  (Ti) and  $a^5F(4s^1 3d^7)$  (Fe) states,  $0.806 + 0.875 = 1.681$  eV above the ground state dissociation channel,  $a^3F(\text{Ti}) + a^5D(\text{Fe})$ .<sup>94</sup> Including all of the separated atom states be-

tween the ground separated atom limit and the limit that leads to bond formation for the  $X^1\Sigma^+$  state, there are 9 channels, namely  $\text{Ti}(4s^2 3d^2; a^3F) + \text{Fe}(4s^2 3d^6; a^5D)$ ,  $\text{Ti}(4s^1 3d^3; a^5F) + \text{Fe}(4s^2 3d^6; a^5D)$ ,  $\text{Ti}(4s^2 3d^2; a^1D) + \text{Fe}(4s^2 3d^6; a^5D)$ ,  $\text{Ti}(4s^2 3d^2; a^3F) + \text{Fe}(4s^1 3d^7; a^5F)$ ,  $\text{Ti}(4s^2 3d^2; a^3P) + \text{Fe}(4s^2 3d^6; a^5D)$ ,  $\text{Ti}(4s^1 3d^3; b^3F) + \text{Fe}(4s^2 3d^6; a^5D)$ ,  $\text{Ti}(4s^2 3d^2; a^1G) + \text{Fe}(4s^2 3d^6; a^5D)$ ,  $\text{Ti}(4s^2 3d^2; a^3F) + \text{Fe}(4s^1 3d^7; a^3F)$ , and  $\text{Ti}(4s^1 3d^3; a^5F) + \text{Fe}(4s^1 3d^7; a^5F)$  at 0.0, 0.806, 0.872, 0.875, 1.032, 1.420, 1.475, 1.488, and 1.681 eV, respectively.<sup>94</sup> The number of molecular  $|\Lambda S\rangle$  ( $|\Omega\rangle$ ) states emanating from each channel is 60 (525), 100 (875), 15 (125), 84 (735), 27 (225), 60 (525), 25 (225), 84 (441), and 140 (1225), respectively, a total of 595 (4901). By inspection of the atomic electronic configurations and based on our previous experience,<sup>91–93</sup>  $4s^2$ – $4s^2$  distributions (channels 1, 3, 5, and 7) lead to van der Waals interactions, whereas  $4s^1$ – $4s^2$  configurations (channels 2, 4, 6, and 8) can give rise to 3 electron–2 center weakly bound states. The only “chemically” relevant channel which can lead to strongly bound states is the ninth one, i.e.,  $\text{Ti}(4s^1 3d^3; a^5F) + \text{Fe}(4s^1 3d^7; a^5F)$ , giving rise to 140  $^{2S+1}\Lambda$  states, that is,  $^{1,3,5,7,9}(\Sigma^+[4], \Sigma^-[3], \Pi[6], \Delta[5], \Phi[4], \Gamma[3], \text{H}[2], \text{I})$ .

The above short exposition rationalizes our reservations about the possibility of quantitative all–electron first principles calculations for the 3d– $\text{M}_2$  or 3d– $\text{MM}'$  molecules with today’s technology.

### B. Computational results

Table IV collects our theoretical results and Figure 6 displays potential energy curves of the 10 states investigated in

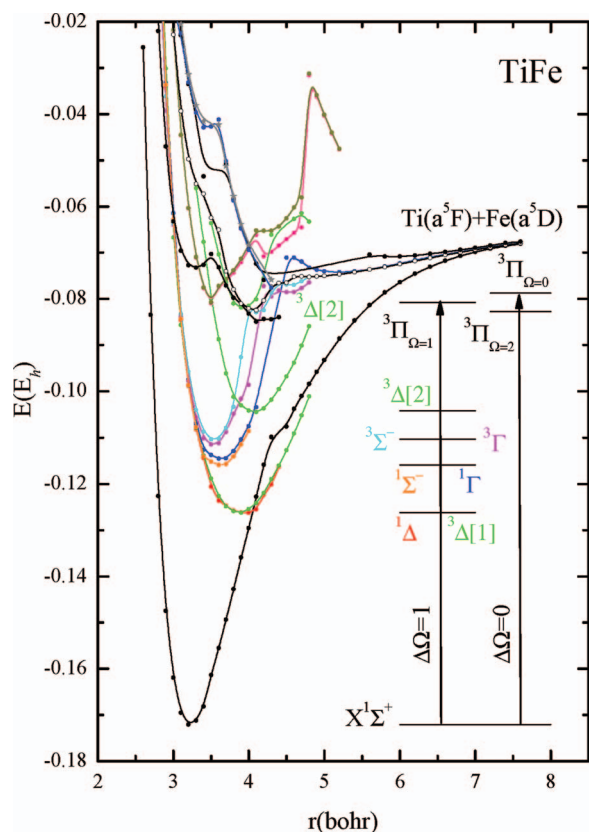


FIG. 6. MRCI potential energy curves for 10 states of the TiFe molecule and corresponding energy level diagram (inset).

this report. We list common molecular constants ( $r_e$ ,  $\omega_e$ ,  $\omega_e x_e$ ,  $T_e$ ), dissociation energies ( $D_e$ ), and permanent electric dipole moments ( $\mu$ ) of the  $^{48}\text{Ti}^{56}\text{Fe}$  isotopomer. Observe the rugged morphology of the potential curves, reflecting the complexity of the electronic structure of the TiFe molecule discussed above.

### 1. $X^1\Sigma^+$

Our calculations, in agreement with the present experimental results, indicate that the ground state of TiFe is  $^1\Sigma^+$ . The dominant equilibrium CASSCF configurations, Mulliken atomic population distributions, relevant molecular orbitals, and total charges ( $q$ ), are

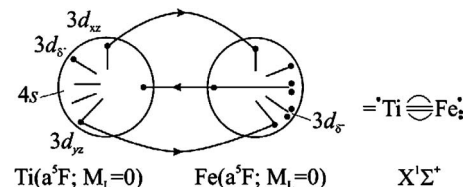
$$|X^1\Sigma^+\rangle \approx 0.69 |1\sigma^2 1\delta_+^2 2\sigma^2 1\pi_x^2 1\pi_y^2 1\delta_-^2\rangle \\ + 0.33 (|1\sigma^2 1\delta_+^2 2\sigma^2 1\pi_x^2 1\pi_y^2 1\delta_- 2\bar{\delta}_-\rangle \\ + |1\sigma^2 1\delta_+ 2\bar{\delta}_+ 2\sigma^2 1\pi_x^2 1\pi_y^2 1\delta_-^2\rangle),$$

where  $\delta_+$  corresponds to the  $\delta_{x^2-y^2}$  orbital and  $\delta_-$  corresponds to the  $\delta_{xy}$  orbital.

$$\text{Ti} : 4s^{1.33} 4p_z^{0.05} 3d_{z^2}^{0.60} 4p_x^{0.03} 3d_{xz}^{0.62} 4p_y^{0.03} 3d_{yz}^{0.62} 3d_{x^2-y^2}^{0.50} 3d_{xy}^{0.50}, \\ q = -0.36 \\ \text{Fe} : 4s^{0.59} 4p_z^{0.03} 3d_{z^2}^{1.34} 4p_x^{0.03} 3d_{xz}^{1.32} 4p_y^{0.03} 3d_{yz}^{1.32} 3d_{x^2-y^2}^{1.47} 3d_{xy}^{1.47}, \\ q = +0.36$$

$$1\sigma \approx (0.71)3d_{z^2}^{\text{Fe}} + (0.38)3d_{z^2}^{\text{Ti}} - (0.31)4s^{\text{Fe}} - (0.26)4s^{\text{Ti}} \\ 2\sigma \approx (0.67)4s^{\text{Ti}} + (0.58)4s^{\text{Fe}} + (0.45)3d_{z^2}^{\text{Fe}} + (0.27)3d_{z^2}^{\text{Ti}} \\ 1\pi \approx (0.79)3d_{\pi}^{\text{Fe}} - (0.46)3d_{\pi}^{\text{Ti}} \\ 1\delta_{\pm} \approx (0.93)3d_{\delta}^{\text{Fe}}, 2\delta_{\pm} \approx (0.93)3d_{\delta}^{\text{Ti}}$$

The atomic populations and the natural orbitals given above suggest a *zeroth* order bonding scheme that can be visualized by the following valence-bond-Lewis diagram.



It should be noted that the 4s atomic orbitals of Ti and Fe are much more extended than the 3d orbitals. In fact, the ratio of the Hartree-Fock radii are  $\langle r_{4s} \rangle / \langle r_{3d} \rangle = 2.6$  (Ti) and 3.0 (Fe).<sup>94</sup> According to this diagram, the bonding interaction can be ascribed to two  $\sigma$  bonds (four electrons coupled into a singlet) and two  $\pi_d$  bonds; the four  $\delta$  electrons are strictly localized on the respective 3d atomic orbitals with no contribution to the bonding. According to the Mulliken analysis, a total of  $\sim 0.4 e^-$  move from Fe to Ti, the result of a  $0.65 e^-$  charge transfer from Ti to Fe along the  $\pi$  frame, and a back  $\sigma$ -transfer of  $\sim 1e^-$ .

The MRCI (+Q) bond distance of the  $X^1\Sigma^+$  state is  $r_e = 1.707$  (1.724) Å (Table IV), in relatively good agreement with the experimental value of  $r_0 = 1.7024(3)$  Å. The calculated adiabatic dissociation energy with respect to the fragments  $\text{Ti}(a^5F) + \text{Fe}(a^5D)$  (2nd channel),  $D_e = 70.6$  (71.3) kcal/mol, is in conformity with the experimental results,  $D \geq 67$  kcal/mol ( $= 2.91$  eV). Notice that both the *in situ* atoms are in their excited configurations  $\text{Ti}(4s^1 3d^3; a^5F)$  and  $\text{Fe}(4s^1 3d^7; a^5F)$  (9th channel), lying experimentally 1.681 eV above the ground state (1st) channel. With respect to the diabatic end products the calculated MRCI (+Q) binding energy is  $D_{\text{diabatic}} = D_{\text{adiabatic}} + \Delta E(9 \leftarrow 2) = 70.6$  (71.3) + 22.5 (23.7) = 93.1 (95.0) kcal/mol. Interestingly, the binding energy calculated by the approximate formula,  $D_e = \omega_e^2 / 4\omega_e x_e$ , is 97.5 kcal/mol. The MRCI (ACPF) electric dipole moment calculated as an expectation value is  $\langle \mu \rangle = 1.96$  (2.12) D. When calculated by the finite-field method, the corresponding MRCI (MRCI + Q) [ACPF] values are 1.74 (1.85) [1.90] D with field strengths ranging from  $10^{-6}$  to  $10^{-5}$  a.u. We recommend  $\mu = 2.0 \pm 0.1$  D, with the positive end on the Fe atom,  $\text{Ti}^-\text{Fe}^+$ .

A density functional theory (DFT) calculation of TiFe has been published by Gutsev *et al.*<sup>55</sup> These workers studied the ground states of all 3d-MM' (M, M' = Sc–Zn) diatomics. For the TiFe ( $X^1\Sigma^+$ ) species, their DFT(BPW91)/6-311+G\* results are:  $r_e = 1.67$  Å,  $D_0 = 94.5$  kcal/mol ( $= 4.1$  eV), and  $\omega_e = 681$   $\text{cm}^{-1}$ ; a sextuple Ti–Fe bond was also suggested.<sup>55</sup>

### 2. $^1\Delta$ , $^3\Delta[1]$

The  $^1\Delta$  and  $^3\Delta[1]$  states have a strongly multireference character, the prevailing feature for both states being a  $\delta^4 \rightarrow \delta^3\sigma^1$  excitation with respect to the  $X^1\Sigma^+$  state. At the

MRCI level the  $^1\Delta$  and  $^3\Delta[1]$  states are strictly degenerate with  $T_e = 10\,923$  and  $10\,929\text{ cm}^{-1}$ , respectively, correlating adiabatically to channel 2; see Figure 6. With respect to the adiabatic atoms,  $D_e(^1\Delta, ^3\Delta[1]) = 39.3\text{ kcal/mol}$ . The calculated bond lengths are  $r_e = 2.096$  ( $^1\Delta$ ) and  $2.06$  ( $^3\Delta[1]$ ) Å, with remarkably small calculated dipole moments as compared to the ground state,  $\langle\mu\rangle = 0.10$  ( $^1\Delta$ ) and  $0.20\text{ D}$  ( $^3\Delta[1]$ ). Observe that for the  $^1\Delta$  state the  $\omega_e$  and  $\omega_e x_e$  molecular constants could not be obtained (Table IV) due to the vagaries of its potential energy curve. It should be mentioned that, quite generally, the construction of potential energy curves for diatomic TiFe led to a variety of technical problems, all related to the extreme density of molecular states (*vide supra*).

### 3. $^1\Sigma^-$ , $^1\Gamma$ , $^3\Gamma$ , $^3\Sigma^-$

The dominant equilibrium CASSCF configurations of these four states above are

$$\begin{aligned} |^1\Sigma_-, ^1\Gamma_+\rangle &\approx 0.55(|1\sigma^2 2\sigma^2 1\delta_+^2 2\delta_+^1 1\pi_x^2 1\pi_y^2 1\delta_-^1\rangle) \\ &\quad \mp (|1\sigma^2 2\sigma^2 1\delta_+^1 1\pi_x^2 1\pi_y^2 1\delta_-^2 2\delta_-^1\rangle), \\ |^3\Sigma_+, ^3\Gamma_-\rangle &\approx 0.57(|1\sigma^2 2\sigma^2 1\delta_+^2 2\delta_+^1 1\pi_x^2 1\pi_y^2 1\delta_-^1\rangle) \\ &\quad \pm (|1\sigma^2 2\sigma^2 1\delta_+^1 1\pi_x^2 1\pi_y^2 1\delta_-^2 2\delta_-^1\rangle), \end{aligned}$$

where the  $\pm$  subscripts on the  $\Sigma$  and  $\Gamma$  symbols correspond to the choice of  $\pm$  in the linear combination that appears in the wavefunction. These four states are all generated from the ground electronic state by a promotion of a  $1\delta$  electron to the  $2\delta$  orbital. The states of the same multiplicity have identical components, the only difference being the sign of the linear combination. The similarity between singlets and triplets is reflected in the similar shapes of their potential energy curves, hence their similar properties. In particular  $r_e$ ,  $D_e$ ,  $\omega_e$ , and  $\mu$  of  $^1\Sigma^-$  and  $^1\Gamma$ , and  $^3\Sigma^-$  and  $^3\Gamma$ , are practically the same. In addition, the ( $^1\Sigma^-$ ,  $^1\Gamma$ ) and ( $^3\Sigma^-$ ,  $^3\Gamma$ ) states are quasidegenerate with MRCI(+Q)  $T_e = [13\,178(10\,732), 13\,463(9964)]$  and  $[14\,161(11\,588), 14\,382(11\,654)]\text{ cm}^{-1}$ , respectively; see Table IV and Figure 6.

### 4. $^3\Delta[2]$

The MRCI(+Q)  $^3\Delta[2] - X^1\Sigma^+$  separation energy is  $15\,697(12\,817)\text{ cm}^{-1}$ , with  $r_e = 2.160\text{ Å}$ , and  $D_e = 25.7\text{ kcal/mol}$  with respect to channel 2, i.e.,  $\text{Ti}(4s^1 3d^3; a^5F) + \text{Fe}(4s^2 3d^6; a^5D)$ . The  $^3\Delta[2]$  state is characterized by a long bond distance,  $\sim 0.50\text{ Å}$  longer than that of the  $X^1\Sigma^+$  state, and a very small dipole moment,  $\langle\mu\rangle = 0.22\text{ D}$ , see Table IV.

### 5. $^3\Pi$ , $^3\Phi$

The  $^3\Pi$  and  $^3\Phi$  states arise from the ground  $^1\Sigma^+$  state primarily by promotion of a  $1\delta$  electron to the  $2\pi$  orbital, with dominant equilibrium configurations of

$$\begin{aligned} |^3\Phi_+, ^3\Pi_-\rangle &\approx 0.60(|1\sigma^2 2\sigma^2 1\delta_+^2 1\pi_x^2 1\pi_y^2 2\pi_y^1 1\delta_-^1\rangle) \\ &\quad \pm (|1\sigma^2 2\sigma^2 1\delta_+^1 1\pi_x^2 2\pi_x^1 1\pi_y^2 1\delta_-^1\rangle) \end{aligned}$$

Here the “+” sign refers to the  $^3\Phi$ , and the “−” to the  $^3\Pi$  state. The two states are strictly degenerate, the MRCI(+Q)

$T_e$  being  $20\,854(17\,185)\text{ cm}^{-1}$  for both states (but see below). Their dissociation energy with respect to channel 2, is  $D_e = 11\text{ kcal/mol}$ , but with an energy barrier with respect to equilibrium ( $r_e = 1.847\text{ Å}$ ) of  $31\text{ kcal/mol}$ ; see Figure 6. The SO interaction splits the  $^3\Pi$  state into three  $\Omega$  components,  $\Omega = 2, 1, 0^\pm$ , with a calculated SO coupling constant  $A = -438\text{ cm}^{-1}$ . This is close to the semiempirical estimate obtained in Sec. IV C for the  $^3\Pi$  state deriving from the  $1\sigma^2 2\sigma^2 1\pi^4 1\delta^3 2\pi^1$  configuration,  $A = -405\text{ cm}^{-1}$  or  $A = -489\text{ cm}^{-1}$  using the molecular orbital coefficients found here, and is not too far from the experimental value of  $A = -329\text{ cm}^{-1}$ . Taking spin-orbit interaction into consideration, the MRCI+Q  $T_e(^3\Pi \leftarrow X^1\Sigma^+) = 17\,185\text{ cm}^{-1}$  becomes  $T_0(\Omega = 1) = T_e + \Delta\omega_e/2 = 17\,080\text{ cm}^{-1}$  and  $T_0(\Omega = 0) = T_e + \Delta\omega_e/2 - A = 17\,518\text{ cm}^{-1}$ . These values are a bit high compared to the experimental values of  $T_0(\Omega = 1, 0) = 15\,852, 16\,183\text{ cm}^{-1}$ , but given the complexity of the molecule, the agreement can be considered to be very good. In addition, these results provide a definitive identification of the upper states of the  $[15.9]^3\Pi_1$  and  $[16.2]^3\Pi_{0^+}$  excited states that are observed in the experiment.

## VI. SUMMARY

The diatomic molecule, TiFe ( $\Delta Z = 4$ ), has been experimentally investigated for the first time, and is found to have a strongly bound  $^1\Sigma^+$  ground state arising from a leading configuration of  $1\sigma^2 2\sigma^2 1\pi^4 1\delta^4$ , with  $r_0 = 1.7024(3)\text{ Å}$ . This bond length is very similar to the nominally sextuply bonded isoelectronic molecule,  $\text{Cr}_2$ , for which  $r_0 = 1.6858\text{ Å}$ .<sup>8</sup> The adiabatic MRCI+Q binding energy of the  $X^1\Sigma^+$  state of TiFe is  $D_e$  ( $D_0 = D_e - \omega_e/2$ ) =  $71.3$  ( $70.5$ ) kcal/mol with an experimental estimate  $D_0 > 67.1\text{ kcal/mol}$ . The molecule has quadruple bonding character comprising two  $\sigma$  and two  $d_\pi$  bonds. The  $\delta$  electrons remain localized on the individual atoms and are not involved in chemical bonds. Although the isoelectronic molecule,  $\text{ScCo}$  ( $\Delta Z = 6$ ), also has a  $^1\Sigma^+$  ground state, its bond length is significantly increased, to  $1.8121(10)\text{ Å}$ .<sup>95</sup>

The  $\Omega = 0^+$  and 1 levels of a  $^3\Pi_1$  excited state arising from the  $1\sigma^2 2\sigma^2 1\pi^4 1\delta^3 2\pi^1$  configuration have been identified in the experiments, in agreement with *ab initio* work that is also reported here. Given the huge density of states present in this molecule, it is remarkable that this state results from a nearly pure electronic configuration, as do the calculated states that arise from the  $1\sigma^2 2\sigma^2 1\pi^4 1\delta^3 2\delta^1$  configuration. As might be expected when the antibonding  $2\pi$  orbital is populated, there is a significant increase in bond length when moving from the ground state to this  $^3\Pi$  state, which has  $r_e \approx 1.885\text{ Å}$  and  $\omega_e \approx 346.9\text{ cm}^{-1}$ , averaged over the  $\Omega = 0^+$  and 1 components.

Further to the blue ( $20\,000$ – $21\,500\text{ cm}^{-1}$ ) a congested region of the spectrum is found in which there is a large number of much more intense transitions. It is argued that ion-pair states corresponding to  $\text{Ti}^+ + \text{Fe}^-$  provide the oscillator strength for transitions in this region, and that this oscillator strength is shared with other nearby states through state mixing induced by configuration interaction and spin-orbit mixing.

## ACKNOWLEDGMENTS

This material is based upon work supported by the National Science Foundation (NSF) under Grant No. CHE-0808984.

- <sup>1</sup>Y. M. Efremov, A. N. Samoilova, and L. V. Gurvich, *Opt. Spectrosc.* **36**, 381–382 (1974).
- <sup>2</sup>E. P. Kuendig, M. Moskovits, and G. A. Ozin, *Nature (London)* **254**, 503–504 (1975).
- <sup>3</sup>W. E. Klotzbuecher and G. A. Ozin, *J. Am. Chem. Soc.* **100**, 2262–2264 (1978).
- <sup>4</sup>M. J. Pellin and D. M. Gruen, *J. Chem. Phys.* **79**, 5887–5893 (1983).
- <sup>5</sup>D. P. DiLella, W. Limm, R. H. Lipson, M. Moskovits, and K. V. Taylor, *J. Chem. Phys.* **77**, 5263–5266 (1982).
- <sup>6</sup>M. Moskovits, W. Limm, and T. Mejean, *J. Phys. Chem.* **89**, 3886–3890 (1985).
- <sup>7</sup>M. Moskovits, W. Limm, and T. Mejean, *J. Chem. Phys.* **82**, 4875–4879 (1985).
- <sup>8</sup>V. E. Bondybey and J. H. English, *Chem. Phys. Lett.* **94**, 443–447 (1982).
- <sup>9</sup>S. J. Riley, E. K. Parks, L. G. Pobo, and S. Wexler, *J. Chem. Phys.* **79**, 2577–2582 (1983).
- <sup>10</sup>D. L. Michalopoulos, M. E. Geusic, S. G. Hansen, D. E. Powers, and R. E. Smalley, *J. Phys. Chem.* **86**, 3914–3916 (1982).
- <sup>11</sup>S. M. Casey, P. W. Villalta, A. A. Bengali, C. L. Cheng, J. P. Dick, P. T. Fenn, and D. G. Leopold, *J. Am. Chem. Soc.* **113**, 6688–6689 (1991).
- <sup>12</sup>M. M. Goodgame and W. A. Goddard III, *J. Phys. Chem.* **85**, 215–217 (1981).
- <sup>13</sup>M. M. Goodgame and W. A. Goddard III, *Phys. Rev. Lett.* **48**, 135–138 (1982).
- <sup>14</sup>P. M. Atha and I. H. Hillier, *Mol. Phys.* **45**, 285–293 (1982).
- <sup>15</sup>J. Bernhole and N. A. W. Holzwarth, *Phys. Rev. Lett.* **50**, 1451–1454 (1983).
- <sup>16</sup>R. A. Kok and M. B. Hall, *J. Phys. Chem.* **87**, 715–717 (1983).
- <sup>17</sup>S. P. Walch, C. W. Bauschlicher, Jr., B. O. Roos, and C. J. Nelin, *Chem. Phys. Lett.* **103**, 175–179 (1983).
- <sup>18</sup>B. Delley, A. J. Freeman, and D. E. Ellis, *Phys. Rev. Lett.* **50**, 488–491 (1983).
- <sup>19</sup>A. D. McLean and B. Liu, *Chem. Phys. Lett.* **101**, 144–148 (1983).
- <sup>20</sup>N. A. Baykara, B. N. McMaster, and D. R. Salahub, *Mol. Phys.* **52**, 891–905 (1984).
- <sup>21</sup>B. Delley, *Phys. Rev. Lett.* **55**, 2090 (1985).
- <sup>22</sup>G. P. Das and R. L. Jaffe, *Chem. Phys. Lett.* **109**, 206–211 (1984).
- <sup>23</sup>M. M. Goodgame and W. A. Goddard III, *Phys. Rev. Lett.* **54**, 661–664 (1985).
- <sup>24</sup>E. Radzio, J. Andzelem, and D. R. Salahub, *J. Comput. Chem.* **6**, 533–537 (1985).
- <sup>25</sup>K. W. Richman and E. A. McCullough, Jr., *J. Chem. Phys.* **87**, 5050–5051 (1987).
- <sup>26</sup>E. Miyoshi and Y. Sakai, *J. Comput. Chem.* **9**, 719–727 (1988).
- <sup>27</sup>G. E. Scuseria and H. F. Schaefer III, *Chem. Phys. Lett.* **174**, 501–503 (1990).
- <sup>28</sup>G. E. Scuseria, *J. Chem. Phys.* **94**, 442–447 (1991).
- <sup>29</sup>K. Andersson, B. O. Roos, P. A. Malmqvist, and P. O. Widmark, *Chem. Phys. Lett.* **230**, 391–397 (1994).
- <sup>30</sup>C. W. Bauschlicher, Jr. and H. Partridge, *Chem. Phys. Lett.* **231**, 277–282 (1994).
- <sup>31</sup>L. Visscher, H. DeRaedt, and W. C. Nieuwpoort, *Chem. Phys. Lett.* **227**, 327–336 (1994).
- <sup>32</sup>K. Andersson, *Chem. Phys. Lett.* **237**, 212–221 (1995).
- <sup>33</sup>K. E. Edgecombe and A. D. Becke, *Chem. Phys. Lett.* **244**, 427–432 (1995).
- <sup>34</sup>B. O. Roos and K. Andersson, *Chem. Phys. Lett.* **245**, 215–223 (1995).
- <sup>35</sup>I. Panas, *Mol. Phys.* **89**, 239–246 (1996).
- <sup>36</sup>H. Stoll and H.-J. Werner, *Mol. Phys.* **88**, 793–802 (1996).
- <sup>37</sup>H. Dachsel, R. J. Harrison, and D. A. Dixon, *J. Phys. Chem. A* **103**, 152–155 (1999).
- <sup>38</sup>E. J. Thomas, J. S. Murray, C. J. O'Connor, and P. Politzer, *J. Mol. Struct.: THEOCHEM* **487**, 177–182 (1999).
- <sup>39</sup>C. J. Barden, J. C. Rienstra-Kiracofe, and H. F. Schaefer III, *J. Chem. Phys.* **113**, 690–700 (2000).
- <sup>40</sup>S. Yanagisawa, T. Tsuneda, and K. Hirao, *J. Chem. Phys.* **112**, 545–553 (2000).
- <sup>41</sup>N. Desmarais, F. A. Reuse, and S. N. Khanna, *J. Chem. Phys.* **112**, 5576–5584 (2000).
- <sup>42</sup>E. A. Boudreaux and E. Baxter, *Int. J. Quantum Chem.* **85**, 509–513 (2001).
- <sup>43</sup>G. L. Gutsev and C. W. Bauschlicher, *J. Phys. Chem. A* **107**, 4755–4767 (2003).
- <sup>44</sup>M. Valiev, E. J. Bylaska, and J. H. Weare, *J. Chem. Phys.* **119**, 5955–5964 (2003).
- <sup>45</sup>E. A. Boudreaux and E. Baxter, *Int. J. Quantum Chem.* **100**, 1170–1178 (2004).
- <sup>46</sup>P. Celani, H. Stoll, H. J. Werner, and P. J. Knowles, *Mol. Phys.* **102**, 2369–2379 (2004).
- <sup>47</sup>L. Rajchel, P. S. Zuchowski, J. Klos, M. M. Szczesniak, and G. Chalasinski, *J. Chem. Phys.* **127**, 244302/1–244302/10 (2007).
- <sup>48</sup>M. Brynda, L. Gagliardi, and B. O. Roos, *Chem. Phys. Lett.* **471**, 1–10 (2009).
- <sup>49</sup>Y. Kitagawa, Y. Nakanishi, T. Saito, T. Kawakami, M. Okumura, and K. Yamaguchi, *Int. J. Quantum Chem.* **109**, 3315–3324 (2009).
- <sup>50</sup>T. Mueller, *J. Phys. Chem. A* **113**, 12729–12740 (2009).
- <sup>51</sup>Y. Kurashige and T. Yanai, *J. Chem. Phys.* **135**, 094104/1–094104/9 (2011).
- <sup>52</sup>F. Ruiperez, F. Aquilante, J. M. Ugalde, and I. Infante, *J. Chem. Theory Comput.* **7**, 1640–1646 (2011).
- <sup>53</sup>K. Hongo and R. Maezono, *Int. J. Quantum Chem.* **112**, 1243–1255 (2012).
- <sup>54</sup>K. P. Huber and G. Herzberg, *Constants of Diatomic Molecules* (Van Nostrand Reinhold, New York, 1979).
- <sup>55</sup>G. L. Gutsev, M. D. Mochena, P. Jena, C. W. Bauschlicher, Jr., and H. Partridge III, *J. Chem. Phys.* **121**, 6785–6797 (2004).
- <sup>56</sup>O. Krechkivska and M. D. Morse, “ZrFe, a sextuply-bonded diatomic transition metal?” *J. Phys. Chem. A* (in press).
- <sup>57</sup>W. C. Wiley and I. H. McLaren, *Rev. Sci. Instrum.* **26**, 1150–1157 (1955).
- <sup>58</sup>S. Gerstenkorn and P. Luc, *Atlas du Spectre d’Absorption de la Molécule d’Iode entre 14,800–20,000 cm<sup>-1</sup>* (CNRS, Paris, 1978).
- <sup>59</sup>M. D. Morse, in *Methods of Experimental Physics: Atomic, Molecular, and Optical Physics*, Atoms and Molecules Vol. II, edited by F. B. Dunning and R. Hulet (Academic, Orlando, Florida, 1996), pp. 21–47.
- <sup>60</sup>S. Gerstenkorn and P. Luc, *Rev. Phys. Appl.* **14**, 791–794 (1979).
- <sup>61</sup>P. R. Bevington, *Data Reduction and Error Analysis for the Physical Sciences* (McGraw-Hill, New York, 1969).
- <sup>62</sup>N. B. Balabanov and K. A. Peterson, *J. Chem. Phys.* **123**, 064107/1–064107/15 (2005).
- <sup>63</sup>H. J. Werner and P. J. Knowles, *J. Chem. Phys.* **89**, 5803–5814 (1988).
- <sup>64</sup>P. J. Knowles and H. J. Werner, *Chem. Phys. Lett.* **145**, 514–522 (1988).
- <sup>65</sup>S. R. Langhoff and E. R. Davidson, *Int. J. Quantum Chem.* **8**, 61–72 (1974).
- <sup>66</sup>E. R. Davidson and D. W. Silver, *Chem. Phys. Lett.* **52**, 403–406 (1977).
- <sup>67</sup>H.-J. Werner, P. J. Knowles, F. R. Manby, M. Schütz *et al.*, MOLPRO, version 2010.1, a package of *ab initio* programs, 2010, see <http://www.molpro.net>.
- <sup>68</sup>See supplementary material at <http://dx.doi.org/10.1063/1.4738958> for 47 pages of vibronic spectra, tables of rotational lines, and fitted spectroscopic constants.
- <sup>69</sup>H. Lefebvre-Brion and R. W. Field, *The Spectra and Dynamics of Diatomic Molecules* (Elsevier, Amsterdam, 2004).
- <sup>70</sup>B. Simard, M.-A. Lebeault-Dorget, A. Marijnissen, and J. J. ter Meulen, *J. Chem. Phys.* **108**, 9668–9674 (1998).
- <sup>71</sup>L. M. Russon, S. A. Heidecke, M. K. Birke, J. Conceicao, M. D. Morse, and P. B. Armentrout, *J. Chem. Phys.* **100**, 4747–4755 (1994).
- <sup>72</sup>C. A. Arrington, T. Blume, M. D. Morse, M. Doverstål, and U. Sassenberg, *J. Phys. Chem.* **98**, 1398–1406 (1994).
- <sup>73</sup>L. M. Russon, S. A. Heidecke, M. K. Birke, J. Conceicao, P. B. Armentrout, and M. D. Morse, *Chem. Phys. Lett.* **204**, 235–240 (1993).
- <sup>74</sup>J. M. Behm, C. A. Arrington, and M. D. Morse, *J. Chem. Phys.* **99**, 6409–6415 (1993).
- <sup>75</sup>E. M. Spain and M. D. Morse, *J. Phys. Chem.* **96**, 2479–2486 (1992).
- <sup>76</sup>S. Taylor, E. M. Spain, and M. D. Morse, *J. Chem. Phys.* **92**, 2698–2709 (1990).
- <sup>77</sup>G. Herzberg, *Molecular Spectra and Molecular Structure*, Spectra of Diatomic Molecules Vol. I, 2nd ed. (Van Nostrand Reinhold, New York, 1950).
- <sup>78</sup>C. L. Pekeris, *Phys. Rev.* **45**, 98–103 (1934).
- <sup>79</sup>L. Veseth, *Theor. Chim. Acta* **18**, 368–384 (1970).
- <sup>80</sup>J. Simons and J. Nichols, *Quantum Mechanics in Chemistry* (Oxford University Press, New York, 1997).



- <sup>81</sup>V. E. Bondybey, G. P. Schwartz, and J. H. English, *J. Chem. Phys.* **78**, 11–15 (1983).
- <sup>82</sup>G. A. Bishea, N. Marak, and M. D. Morse, *J. Chem. Phys.* **95**, 5618–5629 (1991).
- <sup>83</sup>G. A. Bishea, J. C. Pinegar, and M. D. Morse, *J. Chem. Phys.* **95**, 5630–5645 (1991).
- <sup>84</sup>G. A. Bishea and M. D. Morse, *J. Chem. Phys.* **95**, 5646–5659 (1991).
- <sup>85</sup>E. M. Spain, J. M. Behm, and M. D. Morse, *Chem. Phys. Lett.* **179**, 411–416 (1991).
- <sup>86</sup>J. B. Hopkins, P. R. R. Langridge-Smith, M. D. Morse, and R. E. Smalley, *J. Chem. Phys.* **78**, 1627–1637 (1983).
- <sup>87</sup>M. D. Morse, in *Advances in Metal Semiconductor Clusters*, edited by M. A. Duncan (JAI Press, Greenwich, CT, 1993), Vol. 1, pp. 83–121.
- <sup>88</sup>W. C. Ermler, Y. S. Lee, and K. S. Pitzer, *J. Chem. Phys.* **70**, 293–298 (1979).
- <sup>89</sup>J. E. Sohl, Y. Zhu, and R. D. Knight, *J. Opt. Soc. Am. B* **7**, 9–14 (1990).
- <sup>90</sup>H. Hotop and W. C. Lineberger, *J. Phys. Chem. Ref. Data* **14**, 731–750 (1985).
- <sup>91</sup>A. Kalesos, I. G. Kaplan, and A. Mavridis, *J. Chem. Phys.* **132**, 024309/1–024309/7 (2010).
- <sup>92</sup>A. Kalesos and A. Mavridis, *J. Chem. Phys.* **135**, 134302/1–134302/8 (2011).
- <sup>93</sup>D. Tzeli, U. Miranda, I. G. Kaplan, and A. Mavridis, *J. Chem. Phys.* **129**, 154310/1–154310/8 (2008).
- <sup>94</sup>Y. Ralchenko, A. E. Kramida, J. Reader, and A. N. A. Team, NIST Atomic Spectra Database, version 4, National Institute of Standards and Technology, Gaithersburg, MD, 2011.
- <sup>95</sup>R. Nagarajan and M. D. Morse, *J. Chem. Phys.* **127**, 074304/1–074304/8 (2007).